II. COOPER PAIRS

The pairing interaction correlates pairs of nucleons moving in time reversal states over lengths of the order of $\xi = \hbar v_F/E_{corr}$, much larger than nuclear dimensions (cf. e.g. [3]), in keeping with the fact that the associated two–nucleon correlation energy is $E_{corr} \approx 0.5$–2 MeV. These extended, strongly overlapping virtual objects, known as Cooper pairs, affect most of the properties of nuclei close to their ground state, as well as of their decay. A textbook example of this last assertion is provided by the exotic decay $^{223}\mathrm{Ra} \rightarrow ^{209}\mathrm{Pb} + ^{14}C$. The measured decay constant $\lambda = 4.3 \times 10^{-16}\mathrm{s}^{-1}$, implies that the wavefunction describing the ground state of the superfluid nucleus ^{223}Ra has a component of amplitude of about 10^{-5} corresponding to a shape closely resembling ^{209}Pb in contact with ^{14}C. But this requirement can be fulfilled only if this exotic, strongly deformed system, is superfluid. In other words, if pairs of nucleons are correlated over distances of the order of 20 fm, sum of the Pb and C diameters [14].

A. Pairing rotational band

Nuclear superfluidity can be studied at profit in terms of the mean field, BCS diagonalization of the pairing Hamiltonian [15], namely,

$$H = H_{sp} + V_p, \tag{1}$$

where

$$H_{sp} = \sum_{\nu} (\epsilon_\nu - \lambda) a^+_\nu a_\nu, \tag{2}$$

while

$$V_p = -\Delta(P^+ + P) - \frac{\Delta^2}{G}, \tag{3}$$

and

$$\Delta = G\alpha_0, \tag{4}$$

is the pairing gap ($\Delta \approx 12\ \mathrm{MeV}/\sqrt{A}$), G ($\approx 25\ \mathrm{MeV}/A$) being the pairing coupling constant [3], and

$$P^+ = \sum_{\nu>0} P^+_\nu = \sum_{\nu>0} a^+_\nu a^+_{\bar{\nu}}, \tag{5}$$

$$P = \sum_{\nu>0} a_{\bar{\nu}} a_\nu, \tag{6}$$

are the pair addition and pair removal operators, a_ν and a^+_ν being single-particle creation and annihilation operators, $(\nu\bar{\nu})$ labeling pairs of time reversal states.

The BCS ground state wavefunction describing the most favorable configuration of pairs able to profit from the pairing interaction, can be written in terms of the product of the occupancy probabilities h_ν for individual pairs,

$$|BCS> = \Pi_\nu((1-h_\nu)^{1/2} + h^{1/2}_\nu a^+_\nu a^+_{\bar{\nu}})|0>, \tag{7}$$

where $|0>$ is the fermion vacuum.

Superfluidity is tantamount to the existence of a finite average value of the operators (5), (6) in this state, that is, to a finite value of the order parameter

$$\alpha_0 = < BCS|P^+|BCS > = < BCS|P|BCS >^*, \tag{8}$$

which is equivalent to Cooper pair condensation. In fact, α_0 gives a measure of the number of correlated pairs in the BCS ground state. While the pairing gap (4) is an important quantity relating theory with experiment, α_0 provides the specific measure of superfluidity. In fact, the matrix elements of the pairing interaction may vanish for specific regions of space, or in the case of specific pairs of time reversal orbits, but this does not necessarily imply a vanishing of the order parameter α_0, nor the obliteration of superfluidity.

In keeping with the fact that Cooper pair tunneling is proportional to $|\alpha_0|^2$, this quantity plays also the role of a ($L = 0$) two-nucleon transfer sum rule, sum rule which is essentially exhausted by the superfluid nuclear $|BCS>$ ground state (see Fig. 3). Within the above context, one can posit that two-nucleon transfer reactions are the specific probes of pairing in nuclei.

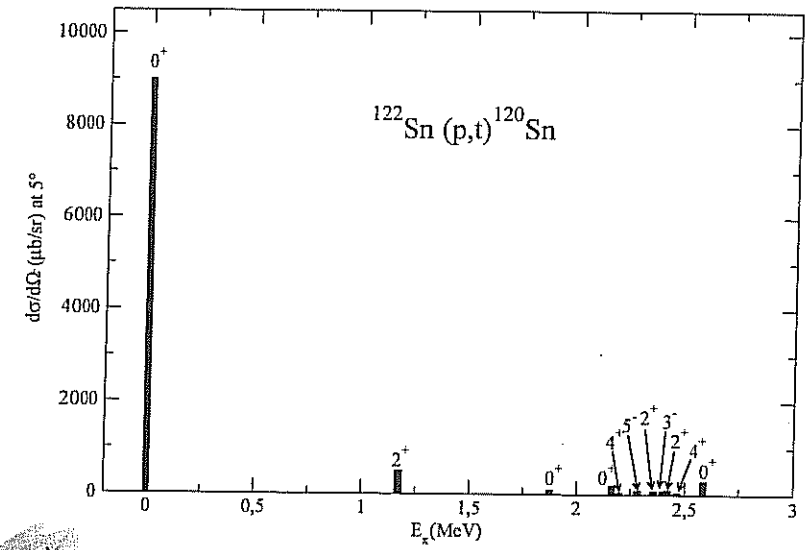

FIG. 1. Excitation function associated with the reaction ^{122}Sn$(p,t)^{120}$Sn(J^π). The absolute experimental value (see ref. *g)* of Table 3) of $d\sigma(J^\pi)/d\Omega|_{5^\circ}$ is given as a function of the excitation energy E_x.

Fluctuations

The BCS solution of the pairing Hamiltonian was recasted by Bogoliubov [16] and Valatin [17] in terms of quasi-particles,

$$\alpha_\nu^+ = U_\nu a_\nu^+ - V_\nu a_{\bar{\nu}}, \tag{9}$$

linear transformation inducing the rotation in (a^+, a)-space which diagonalizes the Hamiltonian (1).

The variational parameters U_ν, V_ν appearing in the above relation indicate that α_ν^+ acting on $|0>$ creates a particle in the state $|\nu>$ which is empty with a probability $U_\nu^2 \equiv (1-h_\nu)$, and annihilates a particle in the time reversal state $|\bar{\nu}>$ (creates a hole) which is occupied with probability $V_\nu^2 (\equiv h_\nu)$. Thus,

$$|BCS> = \Pi_{\nu>0}(U_\nu + V_\nu a_\nu^+ a_{\bar{\nu}}^+)|0>, \tag{10}$$

is the quasiparticle vacuum, as $|BCS> \sim \Pi_\nu \alpha_\nu |0>$, the order parameter being

$$\alpha_0 = \sum_{\nu>0} U_\nu V_\nu. \tag{11}$$

Making use of these results we collect in Table 4 the spectroscopic amplitudes associated with the reactions $^{A+2}$Sn(p,t)^A Sn, for A in the interval 112-126, as well as the spectroscopic amplitudes of other pairing modes (see below as well as [18, 19]).

The BCS number and gap equations are,

$$N = 2\sum_{\nu>0} V_\nu^2, \tag{12}$$

$$\frac{1}{G} = \sum_{\nu>0} \frac{1}{2E_\nu}, \tag{13}$$

where

$$V_\nu = \frac{1}{\sqrt{2}}\left(1 - \frac{\epsilon_\nu - \lambda}{\epsilon_\nu}\right)^{1/2}, \tag{14}$$

$$U_\nu = \frac{1}{\sqrt{2}}\left(1 + \frac{\epsilon_\nu - \lambda}{\epsilon_\nu}\right)^{1/2}, \tag{15}$$

while the quasiparticle energy is defined as

$$E_\nu = \sqrt{(\epsilon_\nu - \lambda)^2 + \Delta^2}. \tag{16}$$

Pairing rotations

The phase of the ground state BCS wavefunction may be chosen so that $U_\nu = |U_\nu| = U'_\nu$ is real and $V_\nu = V'_\nu e^{2i\phi}$ ($V'_\nu \equiv |V_\nu|$). Thus [15, 20, 21],

$$|BCS(\phi)>_{\mathcal{K}} = \Pi_{\nu>0}(U'_\nu + V'_\nu e^{-2i\phi} a_\nu^+ a_{\bar{\nu}}^+)|0> = \Pi_{\nu>0}(U'_\nu + V'_\nu a_\nu^{'+} a_{\bar{\nu}}^{'+})|0> = |BCS(\phi=0)>_{\mathcal{K}'}, \tag{17}$$

where $a_\nu^{'+} = e^{-i\phi} a_\nu^+$ and $a_{\bar{\nu}}^{'+} = e^{-i\phi} a_{\bar{\nu}}^+$. This is in keeping with the fact that a_ν^+ and $a_{\bar{\nu}}^+$ are single-particle creation operators which under gauge transformations (rotations in the 2D-gauge space of angle ϕ) induced by the operator $G(\phi) = e^{-i\hat{N}(\phi)}$ and connecting the intrinsic and the laboratory frames of reference $\mathcal{K}'$ and $\mathcal{K}$ respectively, behave according to $a_\nu^{'+} = \mathcal{G}(\phi) a_\nu^+ \mathcal{G}^{-1}(\phi) = e^{-i\phi} a_\nu^+$ and $a_{\bar{\nu}}^{'+} = \mathcal{G}(\phi) a_{\bar{\nu}}^+ \mathcal{G}^{-1}(\phi) = e^{-i\phi} a_{\bar{\nu}}^+$, a consequence of the fact that $\hat{N}$ is the number operator and that $[\hat{N}, a_\nu^+] = a_\nu^+$.

The fact that the mean field ground state ($|BCS(\phi)>_{\mathcal{K}}$) is a product of operators - one for each pair state - acting on the vacuum, implies that (17) represents an ensemble of ground state wavefunctions averaged over systems with $...N-2, N, N+2...$ even number of particles. In fact, (17) can also be written in the form

	^{112}Sn	^{114}Sn	^{116}Sn	^{118}Sn	^{120}Sn	^{122}Sn	^{124}Sn
$1d_{5/2}$	0.664	0.594	0.393	0.471	0.439	0.394	0.352
$0g_{7/2}$	0.958	0.852	0.542	0.255	0.591	0.504	0.439
$2s_{1/2}$	0.446	0.477	0.442	0.487	0.451	0.413	0.364
$1d_{3/2}$	0.542	0.590	0.695	0.706	0.696	0.651	0.582
$0h_{11/2}$	0.686	0.720	1.062	0.969	1.095	1.175	1.222

b)	^{7}Li	^{8}Be
$0s_{1/2}$	0.0575	0.128
$0p_{3/2}$	1.0491	1.076
$1s_{1/2}$	0.2437	0.232
$0p_{1/2}$	0.2111	0.214
$0d_{5/2}$	0.	0.272

c)	$1s_{1/2}$	$0d_{3/2}$	$0f_{7/2}$	$1p_{3/2}$	$1p_{1/2}$	$0f_{5/2}$
^{50}Ca	0.063	0.0894	0.2041	0.9979	0.1628	0.177

d)	$0h_{9/2}$	$1f_{7/2}$	$0i_{13/2}$	$2p_{3/2}$	$1f_{5/2}$	$2p_{1/2}$
^{206}Pb	0.14	0.18	0.28	0.28	0.47	0.75

e)	$0d_{5/2}$	$1s_{1/2}$	$0d_{3/2}$
^{18}O	0.89	0.396	0.223

$$|^{12}\mathrm{Be}(gs)\rangle \begin{cases} |0\rangle + \alpha|(p_{1/2},s_{1/2})_{1^-}\otimes 1^-;0^+\rangle + \beta|(s_{1/2},d_{5/2})_{2^+}\otimes 2^+;0^+\rangle + \gamma|(p_{1/2},d_{5/2})_{3^-}\otimes 3^-;0^+\rangle \\ \alpha = 0.10, \beta = 0.35, \gamma = 0.33, \\ |0\rangle = 0.37|s^2_{1/2}(0)\rangle + 0.50|p^2_{1/2}(0)\rangle + 0.60|d^2_{1/2}(0)\rangle \end{cases}$$

$$|^{11}\mathrm{Li}(gs)\rangle \begin{cases} |0\rangle + \alpha|(p_{1/2},s_{1/2})_{1^-}\otimes 1^-;0^+\rangle + \beta|(s_{1/2},d_{5/2})_{2^+}\otimes 2^+;0^+\rangle \\ \alpha = 0.7, \beta = 0.1 \\ |0\rangle = 0.45|s^2_{1/2}(0)\rangle + 0.55|p^2_{1/2}(0)\rangle + 0.04|d^2_{6/2}(0)\rangle \end{cases}$$

TABLE 2. (a) Two-nucleon spectroscopic amplitudes $< BCS(A)|P_\nu|BCS(A+2) > = \sqrt{(2j_\nu+1)/2}\, U_\nu(A)V_\nu(A+2)$, associated with two-nucleon pick-up reactions connecting the ground states (members of a pairing rotational band) of two superfluid Sn-nuclei $(^{A+2}\mathrm{Sn}(p,t)^{A}\mathrm{Sn}(gs))$. (b) Two-nucleon spectroscopic amplitudes associated with the pair removal modes $|\tau\rangle$ of the $N_0 = 6$ closed shell systems ^{9}Li and ^{10}Be

$$< \tau|P_\nu|N_0 = 6 >= \begin{cases} X_{rem}(\nu),\ \epsilon_\nu \le \epsilon_F \\ Y_{rem}(\nu),\ \epsilon_\nu > \epsilon_F \end{cases}$$

(c) Two-nucleon spectroscopic amplitude associated with the pair addition mode $|a\rangle$ of the closed shell system ^{48}Ca,

$$< a|P^\dagger_\nu|N_0 = 20 >= \begin{cases} X_{add}(\nu),\ \epsilon_\nu > \epsilon_F \\ Y_{add}(\nu),\ \epsilon_\nu \le \epsilon_F \end{cases}$$

(d) Same as (b) but for the case of the closed shell $N_0 = 126$ nucleus ^{208}Pb. (e) Same as (c) but for the closed shell nucleus ($N_0 = 8$) ^{16}O. In the bottom part of the table, the ground state wavefunctions associated with the pair addition mode of the $N_0 = 6$ closed shell systems ^{10}Be and ^{9}Li are displayed. For details concerning these wavefunctions cf. references [18, 19].

$$|BCS>_{\mathcal{K}}=(\Pi_{\nu>0}U'_\nu)\,(1+...+\frac{e^{-(N-2)i\phi}}{(\frac{N-2}{2})!}\left(\sum_{\nu>0}c_\nu a^+_\nu a^+_{\bar{\nu}}\right)^{\frac{N-2}{2}}+\frac{e^{-Ni\phi}}{(\frac{N}{2})!}\left(\sum_{\nu>0}c_\nu a^+_\nu a^+_{\bar{\nu}}\right)^{\frac{N}{2}}$$

$$+\frac{e^{-(N+2)i\phi}}{(\frac{N+2}{2})!}\left(\sum_{\nu>0}c_\nu a^+_\nu a^+_{\bar{\nu}}\right)^{\frac{N+2}{2}}+...)|0\rangle, \tag{18}$$

where $c_\nu = V'_\nu/U'_\nu$.

Adjusting the Lagrange multiplier λ (chemical potential, see Eqs. (12-16)), one can ensure that the mean number of fermions (Eq. (12)) has the desired value N_0. Summing up, the BCS ground state is a wavepacket in the number of particles. In other words, it is a deformed state in gauge space defining a privileged orientation in this space, and thus an intrinsic coordinate system $\mathcal{K}'$ [22-24]. The magnitude of this deformation is measured by α_0.

Pairing vibrations

All the above arguments, point to a static picture of nuclear superfluidity which results from BCS theory. This is quite natural, as one is dealing with a mean field approximation. The situation is radically changed taking into account the interaction acting among the Cooper pairs (quasiparticles) which has been neglected until now, that is the term $-G(P^+-\alpha_0)(P-\alpha_0)$ left out in the mean field (BCS) approximation leading to (3) [22, 24]. This interaction can essentially be written as (for details see e.g. [4] App. J)

$$H_{residual}=H'_p+H''_p, \tag{19}$$

where

$$H'_p=-\frac{G}{4}\left(\sum_{\nu>0}(U^2_\nu-V^2_\nu)(P^+_\nu+P_\nu)\right)^2, \tag{20}$$

and

$$H''_p=\frac{G}{4}\left(\sum_{\nu>0}(P^+-P)\right)^2. \tag{21}$$

The term H'_p gives rise to vibrations of the pairing gap which (virtually) change particle number in $\pm$ 2 units. The energy of these pairing vibrations cannot be lower than 2Δ. They are, as a rule, little collective, corresponding essentially to almost pure two-quasiparticle excitations (see excited 0^+ states of Fig. 8).

The term H''_p leads to a solution of particular interest, displaying exactly zero energy, thus being degenerate with the ground state. The associated wavefunction is proportional to the particle number operator and thus to the gauge operator inducing an infinitesimal rotation in gauge space. The fluctuations associated with this zero frequency mode diverge, although the Hamiltonian defines a finite inertia. A proper inclusion of these fluctuations (of the orientation angle ϕ in gauge space) restores gauge invariance in the $|BCS(\phi)>_{\mathcal{K}}$ state leading to states with fixed particle number

$$|N_0\rangle \sim \int_0^{2\pi} d\phi e^{iN_0\phi}|BCS(\phi)>_{\mathcal{K}} \sim (\sum_{\nu>0}c_\nu a^+_\nu a^+_{\bar{\nu}})^{N_0/2}|0>. \tag{22}$$

These are the members of the pairing rotational band, e.g. the ground states of the superfluid Sn-isotope nuclei. These states provide the nuclear embodiment of Schrieffer's ensemble of ground state wavefunctions which is at the basis of the BCS theory of superconductivity. This subject has been extensively discussed in the literature (cf. e.g. [20-23] and refs. therein). For a recent discussion within the field of nuclear physics see [11].

Summing up, while the correlations associated with H''_p lead to divergent fluctuations which eventually restore symmetry ($[H_{sp}+H'_p+H''_p,\hat{N}]=0$), H'_p gives essentially rise to non-collective particle number fluctuations, which are essentially pure two-quasiparticle states (cf. [4, 24]).

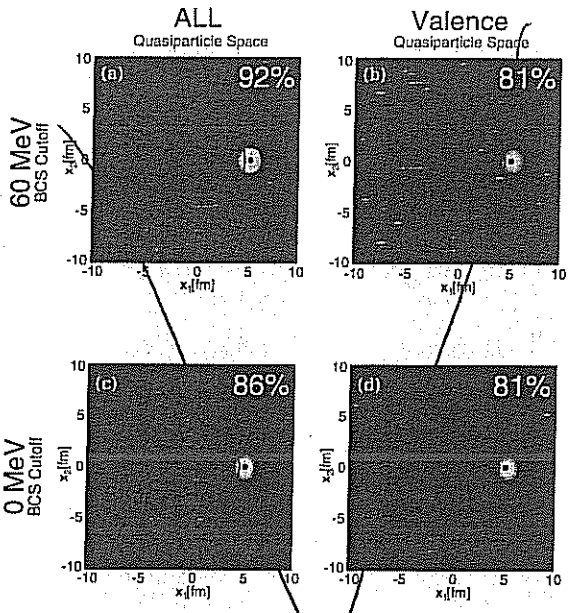

FIG. 8. (Color online) Spatial structure of a two-neutron Cooper pair of ^{120}Sn [see Eqs. (B16), (B17), and (B23)]. The modulus squared wave function $|\Psi_0(\vec{r}_1,\vec{r}_2)|^2 = |\langle\bar{0}|\vec{r}_1,\vec{r}_2\rangle|^2$ (see Tables I and II), multiplied by $16\pi^2 r_1^2 r_2^2$ and normalized to unity, is displayed as a function of the Cartesian coordinates $x_1 = r_2\cos\theta_{12}$ and $x_2 = r_2\sin\theta_{12}$ of particle 2, for a fixed value of $r_1 = x_1 = 5$ fm (black dot) of particle 1, close to the surface of the nucleus (red circle). The numerical percentages correspond to the two-nucleon integrated density in a spherical box of radius 4 fm centered at the coordinates of the fixed particle.

94 μb. Thus, the discrepancies between theory and experiment are bound in the interval $0 \leqslant |\sigma_{\rm exp}(i \to f) - \sigma_{\rm th}(i \to f)|/\sigma_{\rm exp}(i \to f) \leqslant 0.09$, the average discrepancy being 5%.

In Fig. 10 the excited, pairing rotational band associated with the average value of the 0^+ pairing vibrational states with energy $\leqslant$3 MeV, is displayed together with the best parabolic fit. Also given is the relative (p,t) integrated cross section normalized with respect to the gs $\to$ gs transitions, a value which is in all cases $\leqslant$8%, in overall agreement with the single j-shell estimate (see Ref. [10], Appendix H), given in the inset to the figure. The result testifies to the weak cross talk between pairing rotational bands and thus of the robust off-diagonal, long-range order coherence of these modes.

B. Pairing vibrational band in closed-shell nuclei

The expected pairing vibrational spectrum (harmonic approximation, see Refs. [10–12] and references therein) associated with the closed-shell exotic nucleus ^{132}Sn [2,3], up to two-phonon states has been published in Fig. 3 of Ref. [45]. Within this approximation, the one-phonon states are the pair addition $|a\rangle = |{\rm gs}(^{134}{\rm Sn})\rangle$ and pair removal $|\bar{a}\rangle = |{\rm gs}(^{130}{\rm Sn})\rangle$ modes. The two-phonon 0^+ ($|pv(^{132}{\rm Sn})\rangle = |\bar{b}\rangle \otimes |a\rangle = |0^+(^{132}{\rm Sn}; 6.5\ {\rm MeV})\rangle$ pairing vibrational [(2p-2h)-like] state of ^{132}Sn, is predicted at an excitation energy of 6.5 MeV (see Fig. 3). The absolute two-particle transfer differential

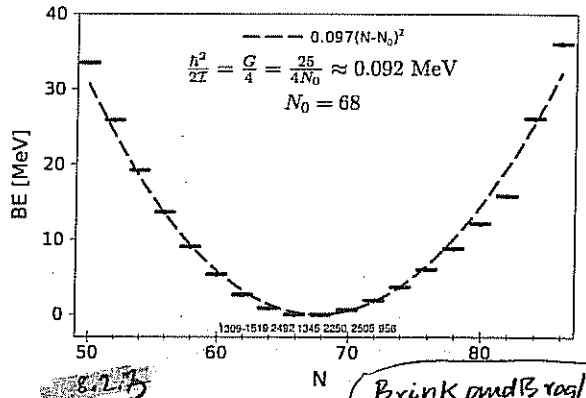

FIG. 9. (Color online) Pairing rotational band along the Sn isotopes. The lines represent the energies calculated according to the expression $BE = B(^{50+N}{\rm Sn}_N) - 8.124N + 46.33$, subtracting the contribution of the single-nucleon addition to the nuclear binding energy obtained by a linear fitting of the binding energies of the whole Sn chain. The estimate of $\hbar^2/2\mathcal{I}$ was obtained using the single j-shell model (see, e.g., Ref. [10], Appendix H). The numbers given on the abscissa are the absolute value of the experimental gs $\to$ gs cross section (in units of μb; see Table II).

cross sections associated with $|a\rangle$ and $|\bar{a}\rangle$, namely,

$$^{134}{\rm Sn}(p,t)^{132}{\rm Sn}({\rm gs}), \quad (E_{\rm CM} = 20\ {\rm MeV}), \tag{41}$$

$$^{132}{\rm Sn}(p,t)^{130}{\rm Sn}({\rm gs}), \quad (E_{\rm CM} = 26\ {\rm MeV}), \tag{42}$$

have been reported in the insets. Using detailed balance the reactions

$$^{130}{\rm Sn}(\bar{t},p)^{132}{\rm Sn}(0^+; 6.5\ {\rm MeV}), \quad (E_{\rm CM} = 20\ {\rm MeV}), \tag{43}$$

$$^{134}{\rm Sn}(p,t)^{132}{\rm Sn}(0^+; 6.5\ {\rm MeV}), \quad (E_{\rm CM} = 26\ {\rm MeV}), \tag{44}$$

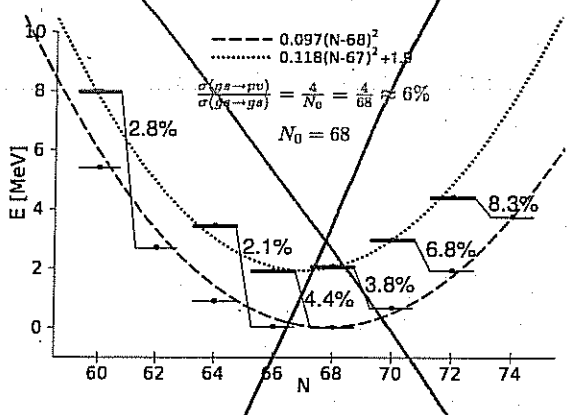

FIG. 10. (Color online) The weighted average energies ($E_{\rm exc} = \sum_i E_i\sigma_i/\sum_i \sigma_i$) of the excited 0^+ states below 3 MeV in the Sn isotopic chain are shown on top of the pairing rotational band, already displayed in Fig. 9. Also indicated is the percentage of cross section for two-neutron transfer to excited states, normalized to the cross sections populating the ground states. The estimate of the ratio of cross sections displayed on top of the figure was obtained making use of the single j-shell model (see, e.g., Ref. [10], Appendix H).

predictions concerning the nuclear structure in general, and two-nucleon spectroscopic amplitudes in particular.

This is in fact the case concerning ^{11}Li and ^{12}Be, two systems studied in much detail with the help of NFT. The two-nucleon transfer spectroscopic amplitudes associated with the reactions ^{1}H(^{11}Li,^{9}Li(J^π))^{3}H ($J^\pi = 3/2^-$ (gs) and $J^\pi = 1/2^-$ ($E^* = 2.69$ MeV)), ^{7}Li(t,p)^{9}Li(gs) and ^{10}Be(t,p)^{12}Be(gs) are collected in Table 1. For details of the calculations of the wavefunctions we refer to [18, 19].

IV. REACTION MECHANISM

Through the single action of the nucleon-nucleon interaction on one nucleon, a two-particle transfer reaction can take place, the second particle being able to follow the first one profitting of the particle-particle (Cooper pair) correlation. Although this is correct, it does not reflect the whole story. To explain why this is so, let us make use of the independent particle model, in which case nucleons do not interact with each other but because of Pauli principle. Nonetheless, also in this limit two-particle transfer can still take place as a first order process in the nucleon-nucleon interaction, the second nucleon going over, profitting this time of the fact that the single-particle wavefunctions are not orthogonal. But this result depends on the single-particle basis used and can thus hardly be correct.

In fact, within the framework of the two-center shell model basis of reaction theory (cf. e.g. [34]), the non-orthogonality term is by definition zero. This is in keeping with the fact that the overlaps $\langle \phi^{(b)}_{a'_1} | \phi^{(A)}_{a_1} \rangle = \langle \phi^{(b)}_{a'_2} | \phi^{(A)}_{a_2} \rangle = 0$. Thus, in the independent particle limit, two-particle simultaneous transfer, in which v acts only once, is non operative.

Consequently, in a non-orthogonal basis like the one used in the present paper, the above parlance implies that, in lowest order in the nucleon-nucleon interaction, there must be two contributions: the simultaneous transfer and another one known as non-orthogonality correction, which exactly cancels the first order in the independent particle limit (cf. e.g. [35] p.424). Because in nuclei, the correlations between Cooper pair partners are weak, cancellation is rather strong, and successive transfer, is, as a rule, the main contribution to two-particle transfer in lowest (second) order in the nucleon-nucleon interaction. It constitutes a further check of the consistency of such a description that in the limit of strong correlations between Cooper pair partners, the non-orthogonality correction is needed to ensure that successive transfer vanishes as the Cooper binding energy becomes large, ensuring simultaneous transfer to be the dominant, lowest order transfer mechanism of the bosonic dinuclear system (see App. A).

The theory of two-nucleon transfer reactions involving superfluid nuclei essentially started with the work of Yoshida [5] who pointed out that the differential cross section connecting the ground states of two superfluid nuclei is proportional to $(\Delta_A/G)^2$, that is $d\sigma_{gs} \to gs \sim (\alpha_0)^2$. Shortly after, Glendenning [36] provided a microscopic description in terms of effective formfactors and DWBA, followed by the seminal work of Bayman [37]. In all these cases use was made of the zero-range approximation (no-recoil effects) and simultaneous transfer was the only process considered.

Work started in the seventies and carrying on to our days (cf. [11–13, 35–91] and App. C), has provided the basis, developed the formalism and worked out the tests for a consistent 2nd order DWBA description of two-nucleon transfer process.

Making use of an implementation ([10], cf. also ref. [11, 51]) of such second order DWBA which includes successive and simultaneous transfer, corrected from non-orthogonality, of the spectroscopic amplitudes collected in Table 1, and of global optical parameters from the literature (see Table 2), a number of two-nucleon transfer absolute differential cross sections have been calculated. They are compared with the experimental findings in Figs. 5 and 6. In Table 3 the corresponding integrated absolute cross sections are collected in comparison with observations. It is fair to state that theory provides an overall account of the experimental findings.

In an attempt at setting the different calculations of the absolute two-particle transfer cross sections on equal footing, global sets of optical parameters, taking also into account spin-orbit terms when reported in the literature, were used. The only exception to this protocol is associated with the analysis of the ^{1}H(^{11}Li,^{9}Li)^{3}He data. In this case, the optical parameters quoted in the paper reporting the inverse kinematic measurement and used to fit the transfer data [19] were employed in the analysis discussed in ref. [50]. This is also in keeping with the fact that it is unlikely that the optical parameters associated with the elastic scattering in the channels p+^{11}Li, d+^{10}Li and t+^{9}Li will smoothly fall within the systematics of a global fit. At the basis of this expectation one finds the high polarizability of ^{11}Li and the fact that ^{10}Li is not bound. The way to proceed in such a case is by calculating microscopically [92–104] ,both the real and imaginary part of the potential, which is likely to be strongly energy (ω-)dependent. This project is, within the present context, to be carried out making use of the nuclear spectroscopic amplitudes [18] and associated modified formfactors used in the analysis of the transfer data in [50] (cf. Fig. 6 and Table III). Such a program and its related outcome constitutes one of the basic open problems in the probing of nuclear correlations with two particle transfer reactions. In any case, it is of notice that in the case of ^{1}H(^{11}Li,^{9}Li)^{3}H both FRESCO and the formalism discussed in the present paper (cf. App. A) give very similar absolute cross sections [49, 50].

Let us now address a second question. Given the importance of successive transfer, one may argue that the deuteron break-up couplings may play a role in the intermediate stage of the reaction. Within this context we refer to Sect.

	V	W	V_{so}	W_d	r_1	a_1	r_2	a_2	r_3	a_3	r_4	a_4
$^{A}\mathrm{Sn}(p,t)^{A-2}\mathrm{Sn}$												
p, $^{A}\mathrm{Sn}$ [a]	50	5	3	6	1.35	0.65	1.2	0.5	1.25	0.7	1.3	0.6
d, $^{A-1}\mathrm{Sn}$ [b]	78.53	12	3.62	10.5	1.1	0.6	1.3	0.5	0.97	0.9	1.3	0.61
t, $^{A-2}\mathrm{Sn}$ [a]	176	20	8	8	1.14	0.6	1.3	0.5	1.1	0.8	1.3	0.6
$^{7}\mathrm{Li}(t,p)^{9}\mathrm{Li}$												
t, $^{7}\mathrm{Li}$ [c]	150.93	12.74	1.0	26.6	1.04	0.72	1.23	1.15	0.54	0.25	1.01	0.83
d, $^{8}\mathrm{Li}$ [b]	89.1	0	3.56	4.8	1.15	0.74			0.97	1.01	1.41	0.65
p, $^{9}\mathrm{Li}$ [d]	56.06	0	4.42	5.32	1.11	0.68			0.87	0.59	1.31	0.52
$^{11}\mathrm{Li}(p,t)^{9}\mathrm{Li}$												
p, $^{11}\mathrm{Li}$ [d]	63.62	0.33	5.69	8.9	1.12	0.68	1.12	0.52	0.89	0.59	1.31	0.52
d, $^{10}\mathrm{Li}$ [b]	90.76	1.6	3.56	10.58	1.15	0.75	1.35	0.64	0.97	1.01	1.4	0.66
t, $^{9}\mathrm{Li}$ [c]	152.47	12.59	1.9	12.08	1.04	0.72	1.23	0.72	0.53	0.24	1.03	0.83
$^{10}\mathrm{Be}(t,p)^{12}\mathrm{Be}$												
t, $^{10}\mathrm{Be}$ [e]	195	18.9	0	0	1.29	0.58	1.37	0.96				
d, $^{11}\mathrm{Be}$ [b]	91.37	1.51	3.58	10.63	1.15	0.75	1.35	0.63	0.97	1.01	1.4	0.67
p, $^{12}\mathrm{Be}$ [e]	90	0	3.5	8.55	1.13	0.57			1.13	0.57	1.13	0.5
$^{48}\mathrm{Ca}(t,p)^{50}\mathrm{Ca}$												
t, $^{48}\mathrm{Ca}$ [f]	144	20	0	0	1.24	0.68	1.35	0.84				
d, $^{49}\mathrm{Ca}$ [b]	85	5	3.	13	1.15	0.9	1.33	0.74	0.8	0.74	1.3	0.8
p, $^{50}\mathrm{Ca}$ [f]	49	10	0	10.5	1.25	0.65	1.25	0.47			1.25	0.47
$^{206}\mathrm{Pb}(t,p)^{208}\mathrm{Pb}$												
t, $^{206}\mathrm{Pb}$ [g]	200	0	0	10	1.4	0.6					1.4	0.6
d, $^{207}\mathrm{Pb}$ [b]	97.78	0	3.56	8	1.15	0.79			0.97	1.01	1.36	0.9
p, $^{208}\mathrm{Pb}$ [g]	55	0	0	11.5	1.25	0.65					1.25	0.47
$^{208}\mathrm{Pb}(^{16}\mathrm{O},^{18}\mathrm{O})^{206}\mathrm{Pb}$												
$^{16}\mathrm{O}$, $^{208}\mathrm{Pb}$ [h]	100	65.4	0	0	1.26	0.45	1.26	0.45				
$^{17}\mathrm{O}$, $^{207}\mathrm{Pb}$ [h]	100	65.4	0	0	1.26	0.45	1.26	0.45				
$^{18}\mathrm{O}$, $^{206}\mathrm{Pb}$ [h]	65	45	0	0	1.35	0.34	1.34	0.33				

TABLE I. Optical potentials used in the calculation of the absolute value of the two-nucleon transfer differential cross sections (see Figs. 5,6 and Table 3). The quantities V, W, V_{SO}, W_d are in MeV while the remaining in fm. The nuclear term of the optical potential was chosen to have the form

$U(r) = -Vf_1(r) - iWf_2(r) - 4iW_d\, g_3(r) - \left(\frac{\hbar}{m_\pi c}\right)^2 V_{so}\frac{g_4(r)}{a_4 r}\mathbf{l}\cdot\mathbf{s}$, with $f_i(r) = \frac{1}{1+e^{(r-R_i)/a_i}}$; $g_i(r) = \frac{e^{(r-R_i)/a_i}}{\left(1+e^{(r-R_i)/a_i}\right)^2}$,

and m_π the pion mass. For (p,t) and (t,p) reactions $R_i = r_i A^{1/3}$, where A is the mass number of the heavy nucleus in the corresponding channel, while for reactions involving heavy nuclei of mass numbers A_a, A_A $R_i = r_i(A_a^{1/3} + A_A^{1/3})$. The Coulomb term is taken to be the electrostatic potential generated by an uniformly charged sphere of radius R_i.

[a] See refs. [105, 110–114].
[b] See ref. [106].
[c] See ref. [107].
[d] See ref. [108].
[e] See ref. [109].
[f] See ref. [62].
[g] See ref. [56].
[h] See ref. [51].

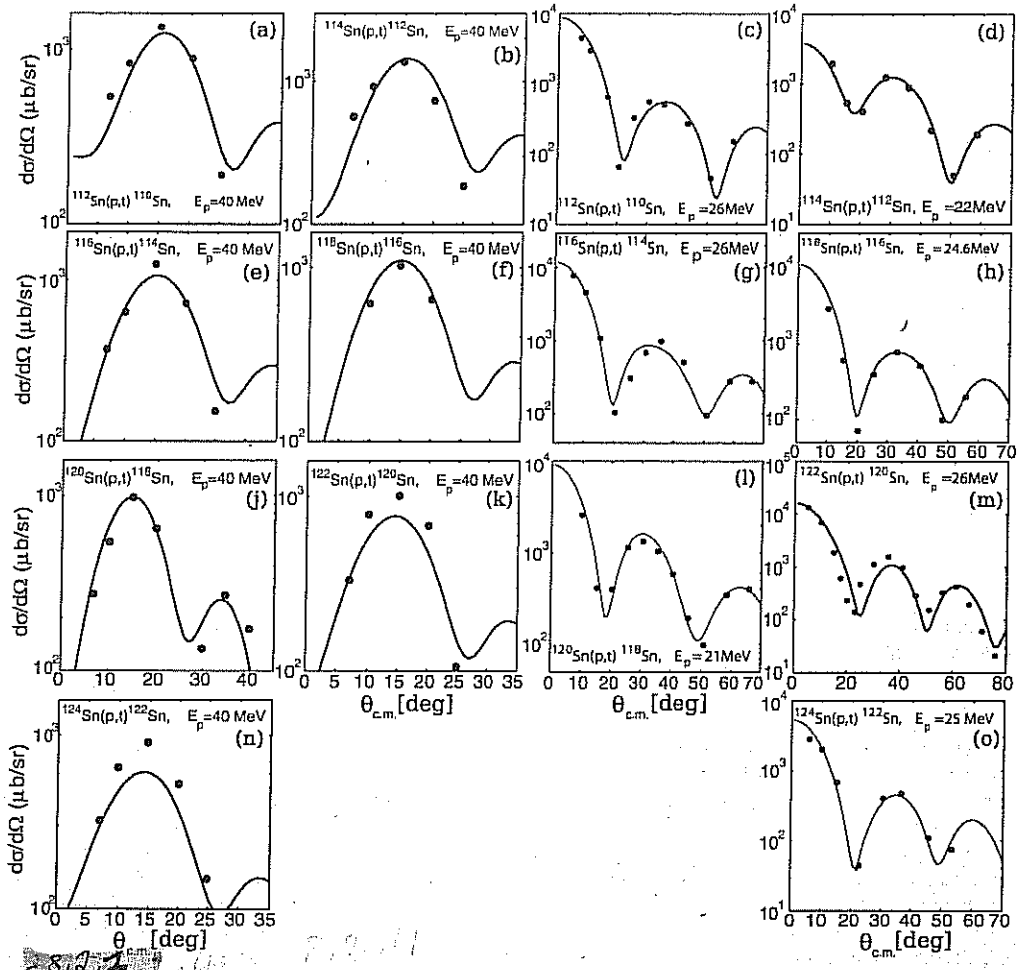

FIG. 9. Predicted absolute differential $^{A+2}$Sn$(p,t)^{A}$Sn(gs) cross sections for bombarding energies $E_p = 40$ MeV (in the two left columns) and 21 MeV $\leqslant E_p \leqslant$ 26 MeV (in the two right columns) in comparison with the experimental data (see Refs. [38–44], respectively).

$E_{\text{cutoff}} = 60$ MeV, discretizing the continuum inside a spherical box of 15 fm of radius. The BCS gap ($\Delta' = 1.47$ MeV; experimental value) and number ($N = 70$) equations lead to $G = 0.18$ MeV and $\lambda = -6.72$ MeV in the first case and $G = 0.05$ MeV and $\lambda = -6.9$ MeV in the second one. The associated Cooper pair probability distributions in r space are essentially identical (see Fig. 8 and Tables I and II). It is then not surprising that they lead to essentially the same absolute value of the two-particle transfer cross section associated with the reaction ^{120}Sn$(p,t)^{118}$Sn(gs).

Let us now repeat the argument, but this time in terms of $\sigma(\text{gs} \to \text{gs}) \sim (\Delta'/G)^2$, as it customarily done since the first publication that introduced it [48]. Because the pairing gap has been fixed to reproduce the experimental value (1.47 MeV), one obtains in the case of $E_{\text{cutoff}} = 0$ MeV $(\Delta'/G)^2 \sim 70$ and $(\Delta'/G)^2 \sim 889$ in the case of $E_{\text{cutoff}} = 60$ MeV. This result emphasizes the problem of working with an expression which contains explicitly the pairing coupling constant.

One could argue that such an objection could also be leveled against the relation $\sigma \sim |\alpha_0|^2$. Note, however, that a (p,t) reaction would hardly feel the effect of contributions far removed from the Fermi surface λ. This is in keeping with the fact that transfer to levels lying far away from λ will be unfavorable owing to Q-value effects. If one argues in terms of the relative distance r between target and projectile ($r \gg R_0$ for continuumlike contributions; $r < R_0$ for deeply boundlike contributions), the outcome is similar. In fact, for large distances the two-particle-transfer form factor vanishes while at small distances the outgoing tritium will experience strong absorption (see Appendix D).

In fact, considering only the contribution to α'_0 arising from the valence orbitals, that is, essentially those contributing to the "naked" vision of the Cooper pair wave functions, one obtains $\alpha'_0 = 2.12$ and $\alpha'_0 = 2.08$, respectively, and thus, a negligible squared relative difference between the two predicted cross sections, namely $(0.04/2.1)^2 \approx 2 \times 10^{-3}$.

Table 8.2.4

Absolute cross section associated with the $^{A+2}$Sn$(p,t)^{A}$Sn(gs) cross sections (i.e., between the members of the Sn-ground state pairing rotational band) calculated as described in the text, in comparison with the experimental findings.

	σ(gs→ gs)	
	Theory	Experiment[c,d]
^{112}Sn$(p,t)^{110}$Sn, $E_p = 26$ MeV	1310[a]	$1309 \pm 200(\pm 14)$[a] $[6° \leqslant \theta \leqslant 62.7°]$
^{114}Sn$(p,t)^{112}$Sn, $E_p = 22$ MeV	1508[a]	$1519.3 \pm 228(\pm 16.2)$[a] $[7.64° \leqslant \theta \leqslant 62.24°]$
^{116}Sn$(p,t)^{114}$Sn, $E_p = 26$ MeV	2267[a]	$2492 \pm 374(\pm 32)$[a] $[4° \leqslant \theta \leqslant 70°]$
^{118}Sn$(p,t)^{116}$Sn, $E_p = 24.6$ MeV	1460[a]	$1345 \pm 202(\pm 24)$[a] $[7.63° \leqslant \theta \leqslant 59.6°]$
^{120}Sn$(p,t)^{118}$Sn, $E_p = 21$ MeV	2440[a]	$2250 \pm 338(\pm 14)$[a] $[7.6° \leqslant \theta \leqslant 69.7°]$
^{122}Sn$(p,t)^{120}$Sn, $E_p = 26$ MeV	2429[a]	$2505 \pm 376(\pm 18)$[a] $[2.5° \leqslant \theta \leqslant 78.5°]$
^{124}Sn$(p,t)^{122}$Sn, $E_p = 25$ MeV	918[a]	$958 \pm 144(\pm 15)$[a] $[4° \leqslant \theta \leqslant 57°]$
^{112}Sn$(p,t)^{110}$Sn, $E_p = 40$ MeV	3349[b]	3715 ± 1114[b]
^{114}Sn$(p,t)^{112}$Sn, $E_p = 40$ MeV	3790[b]	3776 ± 1132[b]
^{116}Sn$(p,t)^{114}$Sn, $E_p = 40$ MeV	3085[b]	3135 ± 940[b]
^{118}Sn$(p,t)^{116}$Sn, $E_p = 40$ MeV	2563[b]	2294 ± 668[b]
^{120}Sn$(p,t)^{118}$Sn, $E_p = 40$ MeV	3224[b]	3024 ± 907[b]
^{122}Sn$(p,t)^{120}$Sn, $E_p = 40$ MeV	2339[b]	2907 ± 872[b]
^{124}Sn$(p,t)^{122}$Sn, $E_p = 40$ MeV	1954[b]	2558 ± 767[b]

[a] μb; the number in parentheses corresponds to the statistical errors; the numbers in square brackets provide the angular range of integration of the absolute two-particle differential cross sections.
[b] μb/sr $[\sum_{i=1}^{N}(d\sigma/d\Omega)$; differential cross section summed over the few, $N = 3$–7 experimental points].
[c] References [38–43]. Zetta - Guazzoni
[d] Reference [44]. Bassani et al

Summing up, because the pair condensed state can be viewed as a coherent state which behaves essentially classically when viewed in terms of its building block (Cooper pair) the description of pairing rotational bands provided by the BCS model in terms of a coupling constant and an energy cutoff can be considered essentially "exact" when probed with two-nucleon transfer processes, reactions which filter the inaccuracies of each individual $U_\nu V_\nu$ component, emphasizing the off-diagonal long-range order provided by the phase coherence (cf. Ref. [49]). In fact, studying nuclear Cooper pair condensation in terms of, e.g., single-nucleon transfer (see, e.g., Refs. [50,51], the individual inaccuracies of the BCS occupation numbers cannot be averaged out. As a consequence, the overall agreement between theory and experiment is much poorer than that reflected by, e.g., the results collected in Table IV. The above arguments provide further evidence of why two-nucleon transfer is the specific probe of pairing superfluidity.

In Fig. 9 a quantity closely related to the Sn isotopes binding energy is reported as a function of the number of neutrons. Also displayed is the best parabolic fit to these energies, a quantity to be compared with

$$E_N = \frac{\hbar^2}{2\mathcal{I}}(N - N_0)^2, \tag{40}$$

namely the energy associated with the members of the pairing rotational band.

A simple estimate of the pairing rotational band moment of inertia is given by the single j-shell model [see, e.g., Ref. [10], Appendix H, $\hbar^2/2\mathcal{I} = G/4 \approx 25/(4N_0)$ MeV].

This estimate turns out to be rather accurate, even beyond expectation. Of notice is that, to the extent that one is discussing properties of a coherent state such as that described by Eq. (12), for which $H_{\rm sp}$ plays a secondary role [see discussion following Eq. (A27) in Appendix A] this is not a surprising result. As can be seen from Fig. 9, the estimate (40) is rather accurate except close to $N = 50$ and $N = 82$, in keeping with the fact that, as discussed before, the pairing deformed picture ($\alpha_0' \neq 0$) breaks down around the closed shell ($\alpha_0' = 0$), where a vibrational regime [associated with the dynamic distortion $\alpha_{\rm dyn}$, see Eq. (18)] is expected to be valid.

Also reported in Fig. 9 are the integrated values of the measured absolute two-particle transfer cross sections. Naively, one would expect a marked constancy of these transitions, in keeping with the fact that the (pairing) rotational model implies a common intrinsic (deformed) state [Cooper pair condensate; see Eq. (12)]. However, owing to the fact that the number of Cooper pairs contributing to the pairing distortion α_0' is rather small (less than 10), one expects strong fluctuations in this quantity ($\Delta\alpha_0'/\alpha_0' \approx \sqrt{7}/7 \approx 0.4$) and consequently in the two-particle transfer cross section ($\sigma \sim \alpha_0'^2$, i.e., fluctuations in σ of the order of 100%).

In keeping with the analogy presented in Fig. 2, in the case of electromagnetic transition between members of a quadrupole rotational band one expects in heavy nuclei fluctuations of the order of $(\sqrt{250}/250)^2$, i.e., less than 1%. Within this context the average value of the absolute experimental cross sections in the energy range $E_p = 21$–26 MeV reported in Table IV is 1762 μb, while the average difference between experimental and predicted values is

App. 8A → (first app. of Ch. 8 (applications 2n-transfer))

Bootstrap particle-phonon mechanism to spontaneously break gauge invariance

(App 8A ①)

Arguably, one can posit that one ~~One~~ now knows how to calculate the absolute differential two-nucleon transfer cross sections (based on NFT structure calculations (Barranco et al (2001))) within experimental errors ~~(quantitative era)~~. One can then use this probe to test nuclear structure predictions by direct comparison with experimental data.

In particular a new embodiment of the Bardeen-Frölich-Pines mechanism to bind Cooper pairs*)

"... It has become fashionable... to assert... that once gauge symmetry is broken the properties of superconductors follow, with no need to inquire into the mechanism by which symmetry is broken... in 1957... the major problem was to show... how... gauge-invariant symmetry of the Lagrangian could be spontaneously broken due to interactions which were themselves gauge invariant". ~~L. Cooper in BCS 50 Years.~~ (Within this context let us quote L. Cooper in BCS:50 Years.)

6.1 Gedanken eksperiment

8A.1

Let us assume that one shines a very intense low-energy neutron beam on a ^{9}Li target. If these neutrons felt only the associated single-particle mean field, they will go by essentially as fast as they came in. ~~In fact, to produce ^{11}Li in its ground state, one has tried rather non-conventional and difficult to justify routes. In particular, one has relaxed the uniqueness of the potential, allowing for a different depth for the $s-$ and the $p-$ orbitals (see e.g. Bertsch), aside from using a conveniently parametrized density dependent pairing interaction, to bind the halo neutrons to the core, with the observed two-neutron separation value $S(2n) \approx 380$ keV.~~ (, these neutrons will be found (cf. Fig. ...))

However, ~~Arguably, a more physically sound alternative is that of allowing the neutrons, which feel a single potential, to be~~ part of the time in ~~the~~ presence of phonon (bosonic) excitations of quadrupole and of (pygmy) dipole character. The first of these collective modes is associated with vibrations of the (even) ^{8}He core, the $p_{3/2}$ proton being a spectator, the second resulting from the sloshing back and forth of the strongly ~~non-local~~ field of two (passing by) neutrons of the beam, together with the neutrons, and against the protons, of the core. (produced also by the field the two neutrons create themselves.)

Such possibility implies that, as discussed above, for a short time, of the order of the traversal time, the two (unbound) neutrons will move in a gas of bosonic excitations, also dipole pigmy resonance. Consequently, they can get dressed becoming heavier (lighter), as well as getting correlated by exchanging information. The first phenomenon is associated with phononic backflow (Pauli principle upflow) leads to ^{10}Li-like quasi-bound ($s-$wave) and resonant ($p-$wave) dressed single-particle states displaying parity inversion. The second phenomenon, mediated by phonon exchange, contributes in a major way to the glue which binds the neutron halo Cooper pair to the ^{9}Li core. The above described bootstrap phonon-exchange mechanism can be viewed as a novel microscopic embodiment of the Bardeen-Frölich-like (Bardeen-Pines-Frölich-) processes to spontaneously break gauge invariance*)

~~Within the framework of effective mean field, the above phenomena can lead to a state dependent effective mass ($m^*_{s_{1/2}} \approx 1.5m$, $m^*_{p_{1/2}} \approx 0.6m$), as well as to an increase of the mean square radius and of the diffusivity of the original potential, quantities which can be parametrized according to~~

$$\langle r^2\rangle^{1/2} = \langle r_0^2\rangle^{1/2}\left(1+\frac{\Delta R}{R_0}\right), \qquad a = a_0\left(1+\frac{\Delta a}{a}\right), \tag{6}$$

~~where ΔR and Δa are proportional to the ZPF associated with the collective particle-hole like modes.~~

*) Bootstrapping or booting. The term is often attributed to Rudolf Erich Raspe's story The surprising Adventures of Baron Münchausen, where the main character pulls himself out of a swamp by his hair. Early 19th century USA: "pull oneself over a fence by one's bootstraps" (footnote)

*) $S_0 NN$-force $V(r_{12}) = \sum_\lambda V_\lambda P_\lambda(\cos\theta)$, $V_\lambda = \frac{2\lambda+1}{4\pi r_1^2}\delta(r_1 - r_2)$ contributions come from high λ-terms ($r_{12} < R/\lambda$). In the case of e.g. ^{11}Li small. (más grande, no se ve)

App 8A (2)

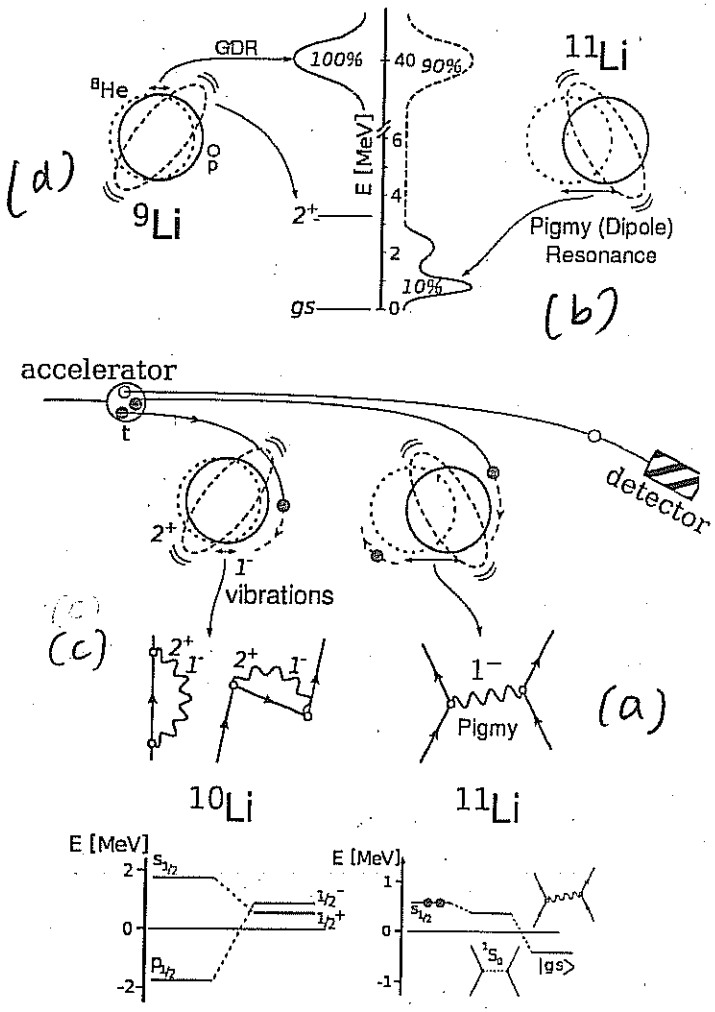

Bootstrap pairing correlations

Figure 8.A.1

Theory (NFT)[5–10] . It provides the rules to work out the interweaving of collective and single–particle degrees of freedom in atomic nuclei. In much the same way as in QED[11–18] , the corresponding couplings and associated renormalization effects arize in the nuclear case from virtual processes, associated with vacuum (ground state) fluctuations, processes which become real in the presence of a fermionic probe.

A typical example of these phenomena in QED is provided by the Lamb shift, namely the splitting between the s,p–orbitals in the hydrogen atom, a phenomenon closely related with the Pauli principle (see Fig. 1).

3. A single Cooper pair nuclear system: ^{11}Li and the single pair tunneling reaction ^{11}Li$(p,t)^{9}$Li

Now, the role of photons in QED is played, in the nuclear case, by collective modes. In the case of the single Cooper pair system ^{11}Li, especially the 0^+ pigmy resonance, namely a low–lying isovector dipole vibration. This is a chunk of the GDR of the core ^{9}Li in which protons and neutrons move out of phase, a mode which is intimately related to the spontaneous symmetry breaking of space inhomogeneity associated with the fact that the center of mass of a finite system like the atomic nucleus, specifies a priviledged position in space, (see Fig. 2).

While $^{9}_{3}$Li$_6$ is bound, $^{10}_{3}$Li$_7$ is not. Nonetheless the single–particle $s_{1/2}$ and $p_{1/2}$ resonances of this system have been studied in detail. It is found that through renormalization processes connected to Pauli–principle–like diagrams as those encountered in connection with the atomic Lamb shifts, the $p_{1/2}$ is shifted to higher energies from that predicted by a standard mean field potential, in keeping with the fact that the quadrupole vibration of the ^{9}Li core has as main component the $(p_{1/2},p_{3/2})_{2^+}$ configuration. Coupling of the $s_{1/2}$ continuum state to the different vibrations of the core lowers the energy of this state (resonance) to energies close, but below that of the $p_{1/2}$ state (parity inversion leading, among other things, to a new "magic number", namely $N = 6$ shell closure, see Fig. 4(I)).

"... Dirk was right ... because his sum–over–histories theory (Feynman path integrals) ... was really supposed to describe physical reality ..."
As a consequence, "... Dirk's electron fields, now known as Feynman diagrams, are the first words in the book of every theorist ..."
F. Dyson, Disturbing the Universe, Harper, New York (1979)

The dressing of single-particle levels by collective vibrations and the renormalization of the bare NN-interaction, in particular of the pairing interaction through the exchange of these modes between nucleons moving in time reversal states lying close to the Fermi energy, play a central role in nuclear structure. (a) In particular, in

Caption to Fig. 8A.1 Bootstrap pairing correlations

most of the glue is provided by the exchange of the

(b) The pigmy resonance

(c,d) bound state

while is lowered to an

also

The exchange of phonons, in

App. 8.A (3)

knocart molecule table App. details

Appendix B

Table 1 PRL

From

"of course" p. 172502-2

to "energy is not conserved, and adiabaticity plays no role"

p. 172502-4

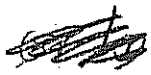

Fig. 2 already in the text

Fig. 2 of PRL

neutrons, with the help of a two-particle transfer process, specific probe of pairing in nuclei [14], [15]. In what follows we shall show, with the help of a quantitative reaction plus nuclear-structure analysis, that the experiment ^{1}H(^{11}Li, ^{9}Li)^{3}H recently carried out at TRIUMF [16], provides direct evidence of phonon exchange between nuclear Cooper pair partners.

To convey the details of such an analysis, which is based on the nuclear-structure description of ^{11}Li reported in [2], nuclear field theory (NFT)–Feynman diagrams (see, e.g., Refs. [17–19] and their generalization to deal with reaction processes [20]) are used (Fig. 1). In Ref. [2], the two halo neutrons correlate through the bare interaction [Fig. 1(a)] and through the exchange of collective vibrations, leading to self-energy (see [21] and references therein) and vertex corrections [boxed processes in Figs. 1(c) and 1(b), respectively; see also Eqs. (1)–(4)]. Solving the associated eigenvalue problem a bound Cooper pair is obtained (S_{2n} = 330 keV).

From the diagrams displayed in Figs. 1(b) and 1(c), it is easy to understand how the virtual propagation of collective vibrations (in the present case 1^- and 2^+ vibrations) can be forced to become a real process: by transferring one or two units of angular momentum in a two-neutron pickup process. In particular, the correlation mechanisms displayed in Figs. 1(b) and 1(c) predict a direct excitation of the quadrupole multiplet of ^{9}Li (see Fig. 1(e), see also [1] Fig. 11.6). On the other hand, if the two-neutron pickup process takes place before the virtual excitation of the vibrational mode, the ground state of ^{9}Li is populated [Fig. 1(d)].

Of course the $1/2^-$ (2.69 MeV) first excited state of ^{9}Li can also be excited through a breakup process in which

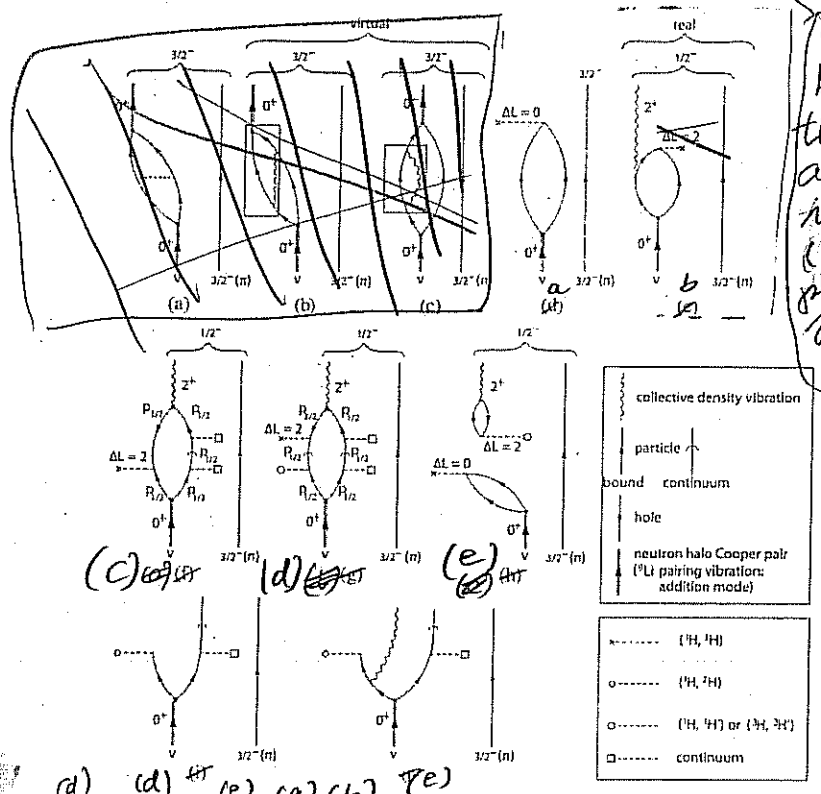

FIG. 1. Representative nuclear field theory–Feynman diagrams associated with correlation process [(a),(b),(c)] and with one- and two-particle pickup reactions [(d),(e) and (b),(c), respectively] of the halo neutrons of ^{11}Li (Cooper pair, indicated in terms of a double arrowed line). Also shown are the possible diagrams associated with other channels (breakup and inelastic) populating the $1/2^-$ (2.69 MeV) state: (c) one of the neutrons is picked up (the other one going into the continuum, i.e., breaking up from the ^{9}Li core) together with a neutron from the $p_{3/2}$ orbital of the ^{9}Li core leading eventually to the excitation of the $1/2^-$ final state [2^+ density mode (wavy line) coupled to the $p_{3/2}(\pi)$], (d) the proton field acting once breaks the Cooper pair forcing one of the halo neutrons to populate a $p_{3/2}$ continuum state (the other one follows suit), while acting for the second time picks up one of the neutrons moving in the continuum and another one from those moving in the $p_{3/2}$ orbital of ^{9}Li eventually leaving the core in the quadrupole mode of excitation. In (e) the two-step transfer to the ^{9}Li ground state plus the inelastic final channel process exciting the $[2^+ \otimes p_{3/2}(\pi)]_{1/2^-}$ state is shown.

one [see Fig. 1(f)], or both neutrons [see Fig. 1(g)] are forced into the continuum for then eventually one of them to fall into the $1p_{3/2}$ orbital of ^{9}Li and excite the quadrupole vibration of the core, in keeping with the fact that the main RPA amplitude of this state is precisely $X(1p_{3/2}^{-1}, 1p_{1/2})$ (≈ 1) (cf. Ref. [2]). The remaining channel populating the first excited state of ^{9}Li is associated with an inelastic process [see Fig. 1(h)]: two-particle transfer to the ground state of ^{9}Li and final state (inelastic scattering) interaction (FSI) between the outgoing triton and ^{9}Li in its ground state, resulting in the inelastic excitation of the $1/2^-$ state.

Making use of the wave functions of Ref. [2] and of software developed on purpose to take into account microscopically all the different processes mentioned above, that is nine different reaction channels and continuum states up to 50 MeV of excitation energy, we have calculated the corresponding transfer amplitude and associated probabilities p_l.

In Table I we display the probabilities $p_l = |S_l^{(c)}|^2$ associated with each of the processes discussed above, where the amplitude $S_l^{(c)}$ is related to the total cross section associated with each of the channels c by the expression [22,23]

$$\sigma_c = \frac{\pi}{k^2}\sum_l (2l+1)|S_l^{(c)}|^2, \qquad (5)$$

k being the wave number of the relative motion between the reacting nuclei.

In keeping with the small values of p_l, in what follows we take into account the interference between the contributions associated with the different reaction paths making use of second order perturbation theory, instead of a coupled channel treatment [24–27]. In particular, in the case of the $1/2^-$ (2.69 MeV) first excited state of ^{9}Li,

$$\frac{d\sigma}{d\Omega}(0) = \frac{\mu^2}{16\pi^2\hbar^4}\left|\sum_l (2l+1)P_l(0)\sum_{c=2}^{5} T_l^{(c)}\right|^2.$$

where μ is the reduced mass and $T_l^{(c)}$ are the transition matrix elements (in the distorted-wave Born approximation [22]) associated with the different channels and for each partial wave.

Making use of all the elements discussed above, multistep transfer (see, e.g., [28–30] as well as [20]), breakup and inelastic channels were calculated, and the results displayed in Figs. 2 and 3 and in Table II. Theory provides an overall account of the experimental findings. In particular, in connection with the $1/2^-$ state, this result essentially emerges from cancellations and coherence effects taking place between the three terms contributing to the multistep two-particle transfer cross section (see Fig. 3), tuned by the nuclear-structure amplitudes associated with the process shown in Fig. 1(c) as well as Eqs. (1)–(4). In fact, and as shown in Figs. 2 and 3, the contributions of inelastic and breakup processes [Figs. 1(f)–1(h), respectively] to the population of the $1/2^-$ (2.69 MeV) first excited state of ^{9}Li are negligible as compared with the process depicted in Fig. 1(e). In the case of the breakup channel [Figs. 1(f) and 1(g)] this is a consequence of the low bombarding energy of the ^{11}Li beam (inverse kinematics), combined with the small overlap between continuum (resonant) neutron $p_{1/2}$ wave functions and bound state wave functions. In the case of the inelastic process [Fig. 1(h)], it is again a consequence of the relative low bombarding energy.

TABLE I. Probabilities p_l associated with the processes described in the text for each partial wave l (note that 4.5, −3 = 4.5×10^{-3}). The different channels are labeled by a channel number c equal to: 1, multistep transfer to the ^{9}Li ground state [Fig. 1(e)]; 2, multistep transfer [Fig. 1(e)], 3, breakup [Fig. 1(g)], 4, breakup [Fig. 1(g)], and 5 inelastic processes [Fig. 1(h)] involved in the population of the 1/2 (2.69 MeV) first excited state of ^{9}Li. Of notice is that the probabilities displayed in columns 1 and 2 result from the (coherent) sum of three amplitudes, namely, those associated with successive, simultaneous and nonorthogonality transfer channels (see also Fig. 3).

l \ c	1	2	3	4	5
0	4.35, −3	1.79, −4	4.81, −6	2.90, −11	3.79, −8
1	3.50, −3	9.31, −4	1.47, −5	1.87, −9	1.09, −6
2	7.50, −4	8.00, −5	2.45, −5	1.25, −8	1.21, −6
3	6.12, −4	9.81, −5	1.51, −6	6.50, −10	2.20, −7
4	1.10, −4	1.18, −5	2.21, −7	4.80, −11	1.46, −8
5	3.65, −5	2.16, −7	7.42, −9	6.60, −13	9.63, −10
6	1.35, −5	6.05, −8	2.88, −10	8.04, −15	1.08, −11
7	4.93, −6	7.78, −8	6.01, −11	4.05, −16	5.26, −13
8	2.43, −6	2.62, −8	7.4, −12	1.26, −17	9.70, −14

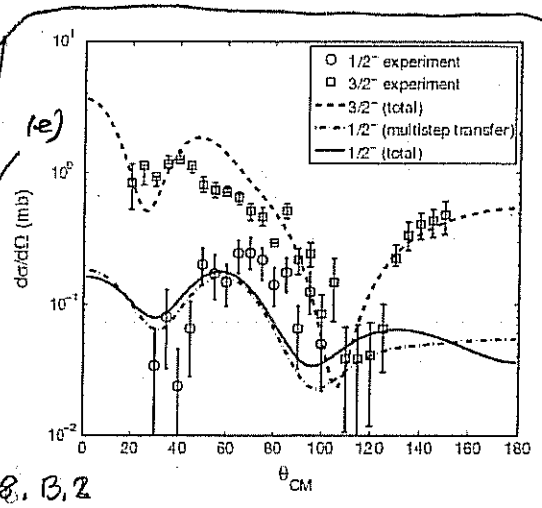

FIG. 2. Experimental [16] and theoretical differential cross sections (including multistep transfer as well as breakup and inelastic channels) of the ^{1}H(^{11}Li, ^{9}Li)^{3}H reaction populating the ground state (3/2) and the first excited state (1/2 ; 2.69 MeV) of ^{9}Li. Also shown (dash-dotted curve) is the differential cross section associated with this state but taking into account only multistep transfer. The optical potentials used are from [16,31].

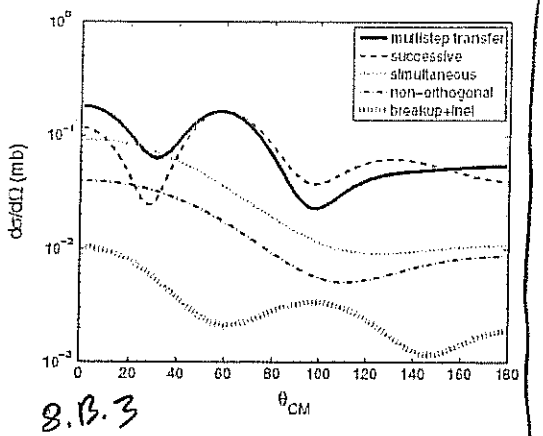

FIG. 8. Successive, simultaneous, and nonorthogonality contributions (prior representation) to the ^{1}H(^{11}Li, ^{9}Li)^{3}H differential cross section associated with the 1/2 state of ^{9}Li, displayed in Fig. 2. Also shown is the (coherent) sum of the breakup ($c = 3$ and 4) and inelastic ($c = 5$) channel contributions.

In fact, the adiabaticity parameters ξ_C, ξ_N [see Eqs. (IV.1.12) and (IV.1.13) of Ref. [20]] associated with Coulomb excitation and inelastic excitation in the $t + {}^9$Li channel are larger than 1, implying an adiabatic cutoff. In other words, the quadrupole mode is essentially only polarized during the reaction but not excited. The situation is quite different in the case of the virtual process displayed in Fig. 1(e). Being this is an off-the-energy shell process, energy is not conserved, and adiabaticity plays no role.

It is worth mentioning that the final states observed in the two-neutron pickup process can, in principle, also be populated in a one-particle pickup process [see Figs. 1(i) and 1(j)].

Summing up, through a unified structure-reaction NFT analysis of the experiment of Tanihata *et al.* [16] we are able to conclude that virtual quadrupole vibration of ^{9}Li, tailored glue of the halo of ^{11}Li, in its process of propagating from one partner of the Cooper pair to the other has been caught in the act by the external pair transfer field produced by the ISAAC-2 facility at TRIUMF, forced to become a real final state and to bring this information to the active target detector MAYA. This is a first in the study of pair correlations in nuclei, providing direct information on the central role polarization effects play in nuclear Cooper pair stabilization.

TABLE II. Integrated two-neutron differential transfer cross sections associated with the ground state [g_s (3/2)] and with the first excited state (2.69 MeV; 1/2) of ^{9}Li in comparison with the data [16]. In the case of the 1/2 state two calculations have been carried out, one making use of the microscopic wave function of Ref. [2] [see Eqs. (1)–(4)] and a second one in which it is (arbitrarily) assumed that $R = 0$ [see Eq. (7)]. That is, that

Discussions with Professor I. Tanihata and Professor R. Kanungo are gratefully aknowledged.

[1] D. Brink and R. A. Broglia, *Nuclear Superfluidity* (Cambridge University Press, Cambridge, U.K., 2005).
[2] F. Barranco *et al.*, Eur. Phys. J. A **11**, 385 (2001).
[3] K. Hagino *et al.*, Phys. Rev. Lett. **99**, 022506 (2007).
[4] T. Myo *et al.*, Prog. Theor. Phys. **108**, 133 (2002).
[5] T. Myo *et al.*, Phys. Rev. C **76**, 024305 (2007).
[6] F. Nunes, Nucl. Phys. A **757**, 519 (2005).
[7] N. V. Mau and J. C. Pacheco, Nucl. Phys. **A607**, 163 (1996).
[8] C. Bachelet *et al.*, Phys. Rev. Lett. **100**, 182501 (2008).
[9] M. Smith *et al.*, Phys. Rev. Lett. **101**, 202501 (2008).
[10] T. Roger *et al.*, Phys. Rev. C **79**, 031603 (2009).
[11] G. F. Bertsch and H. Esbensen, Ann. Phys. (N.Y.) **209**, 327 (1991).
[12] K. Hagino and H. Sagawa, Phys. Rev. C **72**, 044321 (2005).
[13] T. Nakamura *et al.*, Phys. Rev. Lett. **96**, 252502 (2006).
[14] A. Bohr, *Rotational Motion in Nuclei, in Les Prix Nobel en 1975* (Imprimerie Royale Norstedts Tryckeri, Stockholm, 1976), p. 59.
[15] R. A. Broglia, O. Hansen, and C. Riedel, Adv. Nucl. Phys. **6**, 287 (1973).
[16] I. Tanihata *et al.*, Phys. Rev. Lett. **100**, 192502 (2008).
[17] D. R. Bes *et al.*, Nucl. Phys. **A260**, 77 (1976).
[18] B. R. Mottelson, *Elementary Modes of Excitation in Nuclei, Le Prix Nobel en 1975* (Imprimerie Royale Norstedts Tryckeri, Stockholm, 1976), p. 80.
[19] P. F. Bortignon *et al.*, Phys. Rep. **30**, 305 (1977).
[20] R. Broglia and A. Winther, *Heavy Ion Reactions* (Westview Press, Perseus Books, Boulder, 2005), 2nd ed.
[21] C. Mahaux *et al.*, Phys. Rep. **120**, 1 (1985).
[22] G. Satchler, *Introduction to Nuclear Reactions* (McMillan, New York, 1980).
[23] L. Landau and L. Lifshitz, *Quantum Mechanics* (Butterworth-Heinemann, Oxford, 1981), 3rd ed.
[24] R. J. Ascuitto and N. K. Glendenning, Phys. Rev. **181**, 1396 (1969).
[25] T. Tamura *et al.*, Phys. Rev. Lett. **25**, 1507 (1970).
[26] D. T. Khoa and W. von Oertzen, Phys. Lett. B **595**, 193 (2004).

Appendix 8.C

8.C (1)

Modified formfactor associated with the reactions $^{1}H(^{11}Li, ^{9}Li(g.s))^{3}H$ and $^{1}H(^{11}Li, ^{9}Li(1/2^-; 2.69 MeV))^{3}H$ ~~state~~

Gregory

details